

Article

Investigation on Structural, Tensile Properties and Electronic of Mg–X (X = Zn, Ag) Alloys by the First-Principles Method

Yan Gao ¹, Wenjiang Feng ², Chuang Wu ¹, Lu Feng ² and Xiuyan Chen ^{2,*}

¹ Experimental Teaching Center, Shenyang Normal University, Shenyang 110034, China; gaoy@synu.edu.cn (Y.G.)

² College of Physics Science and Technology, Shenyang Normal University, Shenyang 110034, China

* Correspondence: chenxy@synu.edu.cn

Abstract: In order to study the strengthening effect of Mg–X (X = Zn, Ag) alloys, solid solution structures of Mg₅₄, Mg₅₃X₁ and Mg₅₂X₂ (X = Zn, Ag) with atomic contents of 1.8 at.% and 3.7 at.% were established, respectively. The structural stability, tensile properties and electronic properties were investigated by first-principles simulation. The calculated results of cohesive energies show that all solid solution structures were stable under different tensile strains, and Mg₅₂Ag₂ had the best stability. The results of tensile tests show that Zn and Ag atoms promoted the Mg-based alloy's yield strength and tensile strength. In addition, through comparative analyses, we have demonstrated that the tensile property of Mg-based alloys was also affected by solid solubility. Finally, the electronic density of states (DOS) and electron density difference of several solid solution structures were analyzed.

Keywords: first-principles calculation; solid solubility; stability; tensile; electronic



Citation: Gao, Y.; Feng, W.; Wu, C.; Feng, L.; Chen, X. Investigation on Structural, Tensile Properties and Electronic of Mg–X (X = Zn, Ag) Alloys by the First-Principles Method. *Crystals* **2023**, *13*, 820. <https://doi.org/10.3390/cryst13050820>

Academic Editor: Duc Nguyen-Manh

Received: 29 March 2023

Revised: 11 May 2023

Accepted: 11 May 2023

Published: 16 May 2023



Copyright: © 2023 by the authors. Licensee MDPI, Basel, Switzerland. This article is an open access article distributed under the terms and conditions of the Creative Commons Attribution (CC BY) license (<https://creativecommons.org/licenses/by/4.0/>).

1. Introduction

As light metal materials used in industrial production, magnesium alloys are known as a green engineering material with excellent performance characteristics [1–3]. They have the characteristics of low density, good stiffness, high strength-to-weight ratio, high heat dissipation, outstanding casting performance, and high recycling rate. The application of magnesium alloys is always a research hot spot. Magnesium alloys have a wide range of use in the automotive manufacturing, aerospace, 3C electronics, rail transportation and biomedical fields [4–6]. On the one hand, magnesium alloys can meet the performance requirements in practical applications; on the other hand, they are a lightweight material [7–9]. Therefore, magnesium alloys have advantages that other alloy materials cannot compete with. However, the poor ductility and heat resistance of magnesium alloys limit their further development. Researchers have been committed to improving the performance of magnesium alloys, so as to develop new light alloy materials with high performance capacities.

Solid solution strengthening is an effective method used to enhance the mechanical properties of magnesium alloys by adding solid alloying elements dissolved in Mg-based alloys [10,11]. In the solid solutions' structures, the solid atoms replace the magnesium atoms in some areas of the lattice dot matrix, which causes atomic misalignment and lattice distortion [12]. This lattice distortion will prevent dislocation movement and slip, thus concentrating the stress on Mg-based alloys, as a result of which the strength of the magnesium alloys will be improved [13–15]. Zn and Ag are two important alloying elements that are used to improve the properties of magnesium alloys. The atomic structures of Zn and Ag are similar to that of Mg, and have high solid solubility in magnesium alloys; they can also be used as an effective solid solution in Mg-based alloy. The solid solubility of Zn and Ag in magnesium alloys can reach 8.4% and 15.5% at eutectic temperatures. However, it is worth noting that little research has been undertaken on the tensile properties of Mg–Zn

and Mg–Ag alloys at the atomic scale. In particular, comparative studies of their tensile properties at different levels of solid solubility are scarce.

The tensile strength of materials has always been a significant indicator of the solid solution strength [16,17]. Tensile strength can be predicted using the first principle tensile simulation method, after which the solution strengthening effect of alloy elements can be analyzed. The average stress on the structure can be calculated using the first principle tensile simulation method, after which the stresses and strains in the structures can be analyzed. The tensile strength values of structures can be predicted using their stress values at yield. The first principle tensile simulation method was first applied to the calculation of simple crystal structures such as Si, Cu, Al, Mo, Ge, SiC and diamond [18–20], and good prediction results were obtained. These data have helped in guiding experimental operations, and have also helped in saving a lot of money and time.

In the past several years, with the continuous development of computer equipment, it has become possible to assess more complex crystal structures using the first principle tensile simulation method. Zhang et al. [21] found that the maximum stress value of a pure aluminum structure is reached at the tensile strain of 16%, with a value of 9.5×10^3 MPa. Pei et al. investigated the tensile properties of the Al(111)/Al₃Ti(112) interface using first principle tensile simulation. The results indicate that the maximum stress value was 14.38×10^3 MPa, and the Al side was able to absorb most of the deformation energy. Liu et al. [22] studied the solid solution strengthening of Al and Er when used in magnesium alloys through first principles tensile simulations. The study found that Er has a better reinforcement effect. Luo et al. [23] studied the solid solution strengthening effects of Al, Zn and Y on a magnesium matrix using first principles tensile simulations. The strengthening effect of Y is superior to that of other atoms. Wang and Han et al. [24] studied the tensile properties of Mg₅₃Al and Mg₅₁Al₃ using first principles simulation. Collectively, these data indicate that the tensile strength of the Mg-based alloy could be enhanced by covalent bonding between two types of atoms, and the maximum stress value of Mg₅₁Al₃ was increased by 9.4% compared to that of Mg₅₄ using this approach. Wang et al. [25] also investigated the effects of the distribution of Zn and Al atoms on the tensile strength of the magnesium matrix, and found that a uniformly distributed structure had greater tensile strength than a separated one. Wang et al. [25] also studied the relationship between the tensile strength of the magnesium matrix and atomic distribution, and their results have revealed that the tensile strength of the structure was better when the atoms were uniform.

Within the maximum atomic solid solubility range of Zn and Ag atoms in magnesium, the structures of Mg₅₃X₁ (X = Zn, Ag) and Mg₅₂X₂ (X = Zn, Ag) with solid solubilities of 1.8% at.% and 3.7 at.% have been established and studied. First principle tensile simulations were used to test the stability, as well as the stress properties and electronic characteristics, of solid solution structures under 0–20% strains. The effects and mechanisms of the solid solution strengthening of elements Zn and Ag when used in a Mg-based alloy were predicted.

2. Computational Methods

Based on the first principle method with density functional theory (DFT) and generalized gradient approximation (GGA), tensile tests of solid solution structures (Mg₅₃X₁ and Mg₅₂X₂ (X = Zn, Ag)) were carried out. The CASTEP software was used for the calculations, and the exchange correlation functional was PW91. The ultrasoft pseudopotential was used to assess the interaction between the ion nucleus and electron. For the optimization of the solid solution structure, the settings were as follows: the total energy threshold was 1.0×10^{-5} eV/atom, the interatomic force threshold was 3×10^{-2} eV/nm, the maximum internal stress threshold was 0.05×10^3 MPa, and the tolerance deviation threshold was 0.001 Å. Regarding the electronic settings, the cutoff energy and k-point mesh were 340 eV and $3 \times 3 \times 3$, respectively. The tolerance value and maximum number of convergence steps of the SCF self-consistent iteration were 2.0×10^{-6} eV/atom and 150.

Tensile strain was applied along the c-axis of the crystal structures, which was achieved by changing the lattice constant c value in the simulation. During this test, the upper limit

of strain was set to 20%. The strain interval between 6 and 10% strain was 1%, and for the remaining range the strain interval was 2%. After each incremental increase in strain, the solid solution structures need to be geometrically re-optimized, but only the atomic occupation coordinates were optimized, and the lattice constants were not optimized.

In tensile simulations, according to Nielsen-Martin method [26], the average stress acting on the whole cell can be expressed as:

$$\sigma_{\alpha\beta} = \frac{1}{\Omega} \frac{\partial E_{tot}}{\partial \varepsilon_{\alpha\beta}} \quad (1)$$

In the above formula, E_{tot} represents the energy of the entire cell, $\varepsilon_{\alpha\beta}$ represents the strain tensor, and Ω represents the volume. The tensile strain ε was calculated as follows:

$$\varepsilon = \frac{(l_\varepsilon - l_0)}{l_0} \times 100\% \quad (2)$$

In the above formula, l_0 and l_ε are the initial length and tensile length in the c-axis direction of the cell. In addition, in order to reduce the time of calculation, the effect of c-axis stretching on lattice constants in the other two directions was not considered in the stretching simulation process; that is, the influence of the Poisson effect was ignored.

3. Results and Discussion

3.1. Structural Properties

The crystal structure of pure magnesium is shown in Figure 1a. Pure magnesium has an Hcp structure, and its space group is $P6_3/mmc$. The calculated lattice constants are $a = b = 0.3209$ nm and $c = 0.5211$ nm, which are very similar to the results of other simulations [27] wherein $a = b = 0.3195$ nm and $c = 0.5178$ nm, and experimental data [28] wherein $a = b = 0.3210$ nm and $c = 0.5211$ nm. A $3 \times 3 \times 3$ supercell was established through the software's Supercell function [22,29], based on pure magnesium's crystal structure. The $3 \times 3 \times 3$ supercell is shown in Figure 1b. Geometric optimization was performed on the supercell, and the optimized lattice constants are $a = b = 0.9628$ nm and $c = 1.5632$ nm. The supercell contains 54 atoms, hereinafter referred to as Mg_{54} . The structure of the solid solution with an X content of 1.8 at.% is shown in Figure 1c, where the X atom coordinate is $(x = 0.5552, y = 0.4448, z = 0.5802)$, hereinafter referred to as $Mg_{53}X_1$ ($X = Zn, Ag$). The structure of the solid solution with an X content of 3.7 at.% is shown in Figure 1d, where the X atoms coordinates are $(x = 0.5552, y = 0.4448, z = 0.5802)$ and $(x = 0.5552, y = 0.4447, z = 0.2505)$, respectively, hereinafter referred to as $Mg_{52}X_2$ ($X = Zn, Ag$). The atomic positions of $Mg_{52}X_2$ are given in Table 1. During the model establishment process, the energy values of the crystal structures at different positions of the X atoms are calculated and compared, and the most reasonable positions for the placement of the atoms are ultimately determined, and are used as the positions of the X atoms here.

Table 1. The atomic positions of $Mg_{54}X_2$.

Element	Atom Number	Fractional Coordinates of Atoms		
		x	y	z
Mg	1	0.1109	0.2220	0.0829
Mg	2	0.2273	0.1170	0.2505
Mg	3	0.4464	0.2264	0.0865
Mg	4	0.5563	0.1169	0.2505
Mg	5	0.7780	0.2220	0.0828
Mg	6	0.8889	0.1111	0.2497
Mg	7	0.1109	0.5551	0.0842
Mg	8	0.2279	0.4434	0.2505

Table 1. Cont.

Element	Atom Number	Fractional Coordinates of Atoms		
		x	y	z
Mg	9	0.4465	0.5535	0.0865
Mg	10	0.7736	0.5536	0.0865
Mg	11	0.8831	0.4437	0.2505
Mg	12	0.1108	0.8892	0.0842
Mg	13	0.2222	0.7778	0.2501
Mg	14	0.4449	0.8891	0.0842
Mg	15	0.5566	0.7728	0.2505
Mg	16	0.7780	0.8891	0.0829
Mg	17	0.8830	0.7727	0.2505
Mg	18	0.1103	0.2217	0.4169
Mg	19	0.2272	0.1169	0.5823
Mg	20	0.4479	0.2291	0.4172
Mg	21	0.5563	0.1170	0.5823
Mg	22	0.7783	0.2217	0.4170
Mg	23	0.8890	0.1110	0.5833
Mg	24	0.1108	0.5549	0.4171
Mg	25	0.2271	0.4434	0.5823
Mg	26	0.4479	0.5521	0.4173
Mg	27	0.7709	0.5521	0.4172
Mg	28	0.8830	0.4437	0.5823
Mg	29	0.1107	0.8893	0.4170
Mg	30	0.2222	0.7778	0.5828
Mg	31	0.4451	0.8892	0.4171
Mg	32	0.5566	0.7729	0.5823
Mg	33	0.7783	0.8897	0.4169
Mg	34	0.8831	0.7728	0.5823
Mg	35	0.1109	0.2221	0.7501
Mg	36	0.2236	0.1115	0.9170
Mg	37	0.4465	0.2265	0.7474
Mg	38	0.5545	0.1116	0.9171
Mg	39	0.7779	0.2221	0.7501
Mg	40	0.8890	0.1110	0.9170
Mg	41	0.1109	0.5551	0.7489
Mg	42	0.2237	0.4453	0.9171
Mg	43	0.4466	0.5534	0.7474
Mg	44	0.5556	0.4444	0.9170
Mg	45	0.7735	0.5535	0.7474
Mg	46	0.8884	0.4455	0.9171
Mg	47	0.1108	0.8892	0.7489
Mg	48	0.2221	0.7779	0.9170
Mg	49	0.4449	0.8891	0.7489
Mg	50	0.5547	0.7763	0.9171
Mg	51	0.7779	0.8890	0.7501
Mg	52	0.8885	0.7764	0.9170
X	1	0.5552	0.4447	0.2505
X	2	0.5552	0.4448	0.5802

To compare the stability of the two kinds of solid solution structures, the cohesive energy has been calculated. The whole crystal structure's stability depends on the cohesive energy. When the cohesive energy is negative, the structure is stable. In addition, the stability values of different structures can be compared with each other according to the absolute value of cohesive energy. The cohesive energy can be calculated by means of the following formula [30–32]:

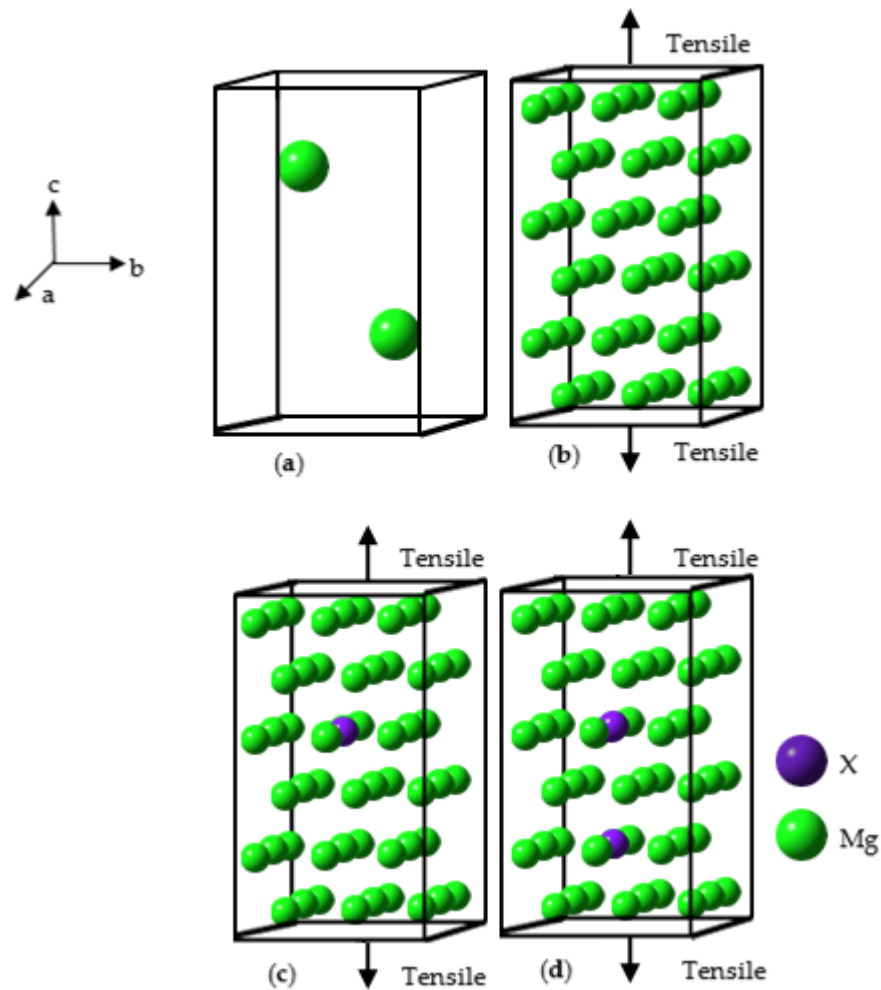


Figure 1. Crystal structure diagram: (a) Mg, (b) Mg₅₄, (c) Mg₅₃X₁, (d) Mg₅₂X₂ (X = Zn, Ag).

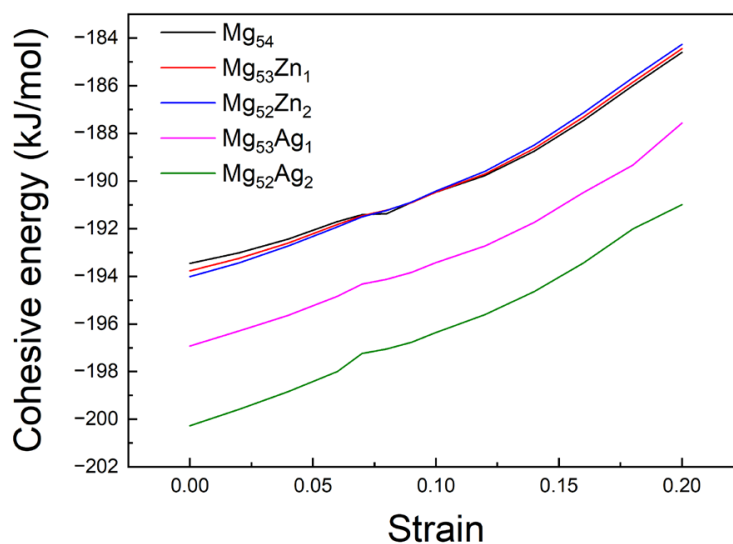
$$E_{coh} = \frac{E_{tot} - N_A E_{atom}^A - N_B E_{atom}^B}{N_A + N_B} \quad (3)$$

In the above formula, E_{coh} and E_{tot} are the cohesive energy and total energy of the structures. E_{atom}^A and E_{atom}^B are the free state energy of Mg and X atoms. The free state energy values of Mg, Zn and Ag atoms are -972.5823 eV/atom, -1708.9884 eV/atom and -1024.9934 eV/atom, respectively. N^A and N^B are the numbers of Mg and X atoms in the structures.

The calculation results of Mg₅₄, Mg₅₃X₁ and Mg₅₂X₂ (X = Zn, Ag) are listed in Table 2. The calculated cohesive energies representing the strain are shown in Figure 2. It can be seen that the cohesive energy values for all the structures are negative in the range of 0–20% strain, which indicates that several structures remain stable during the tensile process. When there is no strain, the absolute order of cohesive energy for the five structures is Mg₅₄ < Mg₅₂Zn₂ < Mg₅₃Ag₁ < Mg₅₂Ag₂, which indicates that the inclusion of Zn and Ag can promote the stability of Mg-based alloys. At the same time, the stability of a Ag-containing solid solution structure is greater than that of one containing Zn. In addition, in the range of 0–20% strain, the cohesive energy values of Mg₅₃X₁ and Mg₅₂X₂ are always negative, but the absolute values are decreased. It can be concluded that with an increase in strain, Mg₅₃X₁ and Mg₅₂X₂ remain stable, but their stability shows a downward trend.

Table 2. The cohesive energy of Mg_{54} , $Mg_{53}X_1$ and $Mg_{52}X_2$ ($X = Zn, Ag$) under different strains.

Strain (%)	E_{coh} , kJ/mol				
	Mg_{54}	$Mg_{53}Zn_1$	$Mg_{52}Zn_2$	$Mg_{53}Ag_1$	$Mg_{52}Ag_2$
0	−193.46	−193.77	−194.01	−196.93	−200.27
2	−193.01	−193.25	−193.44	−196.29	−199.58
4	−192.44	−192.60	−192.73	−195.64	−198.84
6	−191.70	−191.82	−191.92	−194.84	−197.99
7	−191.41	−191.46	−191.50	−194.33	−197.24
8	−191.37	−191.22	−191.23	−194.13	−197.05
9	−190.90	−190.91	−190.89	−193.84	−196.77
10	−190.47	−190.47	−190.42	−193.42	−196.36
12	−189.77	−189.70	−189.59	−192.72	−195.61
14	−188.75	−188.63	−188.49	−191.74	−194.64
16	−187.46	−187.31	−187.13	−190.48	−193.44
18	−186.00	−185.86	−185.66	−189.33	−192.01
20	−184.60	−184.44	−184.26	−187.57	−190.99

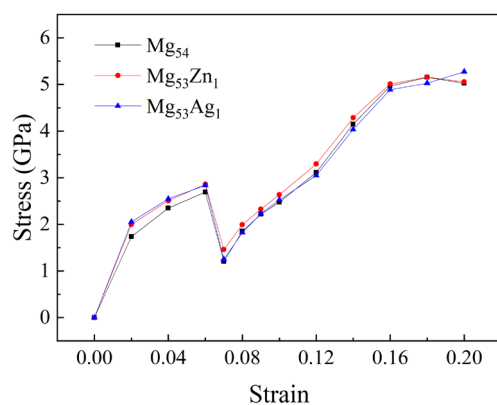
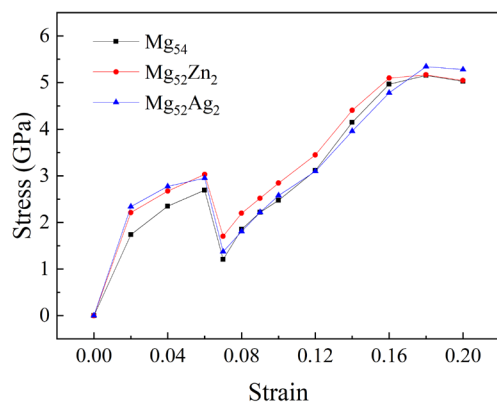
**Figure 2.** The calculated cohesive energies as a function of the strain.

3.2. Tensile Properties

The stress values of Mg_{54} , $Mg_{53}X_1$ and $Mg_{52}X_2$ ($X = Zn, Ag$) under different strains have been calculated using first principle tensile simulations, and are listed in Table 3. The strain should not exceed 20%. For a more intuitive analysis, the corresponding stress–strain curves are shown in Figures 3 and 4. The abscissa represents crystal strain and the ordinate represents stress. It is clear that the types of deformation experienced by the different solid solution structures are the same, as elastic deformation, uneven plastic deformation and uniform plastic deformation successively occurred. In the elastic deformation zone, the solution structure will undergo elastic deformation when stretching, and the structure will return to its original length when stretching ceases. In the non-uniform plastic deformation zone, elastic deformation and plastic deformation will occur simultaneously with the application of stress. Finally, only plastic deformation occurs in the uniform plastic deformation zone.

Table 3. The stress values of Mg_{54} , $Mg_{53}X_1$ and $Mg_{52}X_2$ ($X = Zn, Ag$) under different strains.

Strain (%)	Stress, 10^3 MPa				
	Mg_{54}	$Mg_{53}Zn_1$	$Mg_{52}Zn_2$	$Mg_{53}Ag_1$	$Mg_{52}Ag_2$
0	0.00	0.00	0.00	0.00	0.00
2	1.74	2.00	2.21	2.05	2.34
4	2.35	2.51	2.67	2.55	2.77
6	2.69	2.86	3.03	2.83	2.95
7	1.21	1.46	1.70	1.25	1.37
8	1.85	1.99	2.20	1.82	1.81
9	2.22	2.33	2.52	2.23	2.22
10	2.47	2.63	2.84	2.52	2.58
12	3.11	3.29	3.45	3.05	3.10
14	4.15	4.29	4.41	4.04	3.96
16	4.97	5.01	5.10	4.89	4.78
18	5.15	5.16	5.17	5.03	5.34
20	5.02	5.06	5.04	5.27	5.28

**Figure 3.** Stress–strain curve of materials with Zn and Ag content of 1.8 at. %.**Figure 4.** Stress–strain curve of materials with Zn and Ag contents of 3.7 at. %.

In the elastic deformation area, the stress and strain change in direct proportion to one another, and the image change trend shows a straight line. Figures 3 and 4 show that the elastic deformation areas of several structures are very small, and the strain range is 4–8%. With the increase in strains, non-uniform plastic deformation will rapidly develop. Thereafter, elastic deformation will be accompanied by elastic plastic deformation, after which it will be difficult for this material to completely return to its original length. In industrial production, yield strength is the strength index of a material that can yield, and materials are typically selected for their yield strength. Figure 3 shows that, with the increase in strain, several solid solution structures undergo obvious yielding, accompanied

by the appearance of an upper yield point and a lower yield point. Because lower yield is a stable form of the yield process, the lower yield point is usually selected as the yield strength if the structure shows both upper and lower yield points [33]. It can be seen from Table 3 and Figure 3 that when the solid's solubility is 1.8 at.%, the solid solution structure will have a lower yield point at the strain of 7%, and the yield strengths of Mg_{54} , $Mg_{53}Zn_1$ and $Mg_{53}Ag_1$ will be 1.21×10^3 MPa, 1.46×10^3 MPa and 1.25×10^3 MPa, respectively. When the solid solubility is 1.8 at.%, the inclusion of both Zn and Ag will increase the yield strength of the Mg-based alloy. The yield strengths of the Mg-based alloys with Zn and Ag are increased by 20.67% and 3.31%, respectively, and the strengthening effect of Zn is obviously higher than that of Ag. Additionally, it can be seen from Table 3 and Figure 4 that the yield strengths of $Mg_{52}Zn_2$ and $Mg_{52}Ag_2$ are 1.70×10^3 MPa and 1.37×10^3 MPa, respectively, when the solid solubility is 3.7 at.%, which values are 40.50% and 13.22% higher than those of the Mg-based alloys. It can be seen from the comparison that the inclusion of both Zn and Ag can promote the Mg-based alloy materials' yield strength, and the effect of Zn is more obvious. In addition, the strengthening effect is also affected by the value of solid solubility; in particular, when the solid solubility is 3.7 at.%, the strengthening effect is more obvious.

Tensile strength is another important index that is used to measure the tensile properties of materials. It is the maximum stress that materials can withstand under tension, which can be used to reflect the material's ability to resist damages. When the structure exhibits yielding, a plastic deforming area will appear as the strain continues to increase. In the region of plastic deformation, the stress increases with the increase in strain until the tensile strength is reached. If the strain continues to increase, the stress will drop, which indicates that the structure has been destroyed. The figures show that several solid solution structures of Mg_{54} , $Mg_{53}X_1$ and $Mg_{52}X_2$ ($X = Zn, Ag$) reach their tensile strength value in the plastic deformation zone. When the solid solubility is 1.8 at.%, the tensile strengths of Mg_{54} , $Mg_{53}Zn_1$ and $Mg_{53}Ag_1$ are 5.15×10^3 MPa, 5.16×10^3 MPa and 5.27×10^3 MPa, respectively. The results show that Zn hardly improves the tensile strength of Mg-based alloy materials, while Ag can improve the tensile strength of Mg-based alloys. When the solid solubility is 3.7 at.%, the tensile strengths of $Mg_{52}Zn_2$ and $Mg_{52}Ag_2$ are 5.17×10^3 MPa and 5.34×10^3 MPa, respectively. Further analysis shows that Zn has little effect on the tensile strength of Mg-based alloy materials. Conversely, the strengthening effect of Ag on Mg-based alloy materials is obvious, and will be made more obvious with the increase in solid solubility.

Through the above research, we found that a suitable Ag content can enhance the yield strength and tensile strength of Mg-based alloys, and this strengthening effect is better than that of Zn. The results of this study validate other experimental results. Feng et al. [34] found via microhardness tests that the microhardness of magnesium alloy could be enhanced by adding Ag, and the alloy exhibited good mechanical properties. Ben Hamu et al. [35] found that adding Ag could improve the mechanical properties of Mg–Zn alloys. Zhao et al. [36] found through experiments that Mg–Zn–Ag alloys display their best mechanical properties as the concentration of Ag is changed, with the results being particularly striking for yield strength, ultimate tensile strength, and elongation. From these results, it can be inferred that the method used in this study is correct and feasible for application. Ag belongs to the group of precious metals, which greatly limits the smooth progression of this experiment. This study employed the method of simulated stretching, which not only saves time and costs, but can also be used to obtain reliable data, providing a new path for the study of precious and rare metals.

3.3. Electronic Properties

3.3.1. Density of States

To further understand the stability and strengthening mechanisms of the structures, the densities of different states (total and partial) of $Mg_{52}Zn_2$ and $Mg_{52}Ag_2$ structures have been calculated without the application of strain. The bonding characteristics of the

structures can be inferred through the total density of states and the partial density of states. The total density of states (TDOS) and the partial density of states (PDOS) of $\text{Mg}_{52}\text{Zn}_2$ and $\text{Mg}_{52}\text{Ag}_2$ are depicted in Figures 5 and 6, respectively.

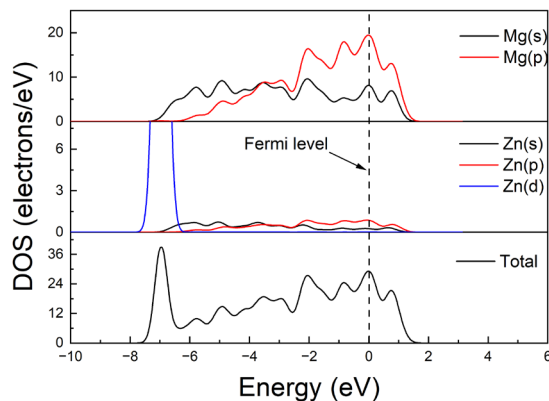


Figure 5. The total and partial density of states of $\text{Mg}_{52}\text{Zn}_2$.

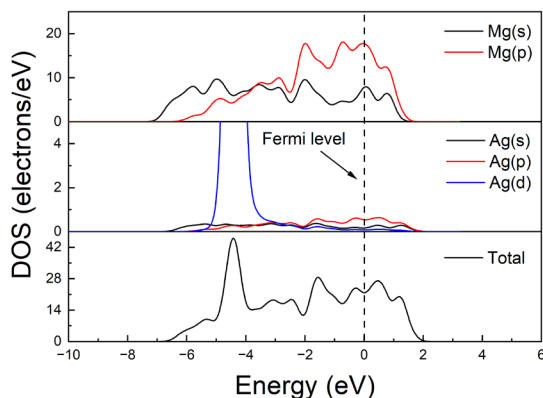


Figure 6. The total and partial density of states of $\text{Mg}_{52}\text{Ag}_2$.

The figures show that at no point does the energy range approach the Fermi level, where there are no electron states, i.e., there is no band gap. The valence and conduction bands overlap, and electrons are delocalized, so the structures exhibit a metallic character. Figure 5 shows that the bonding peaks of $\text{Mg}_{52}\text{Zn}_2$ are mainly distributed in the range from -7.5 to 1.5 eV. Here, the valence band is associated with the valence electrons of Mg s, Mg p, Zn s, Zn p and Zn d orbitals, and the conduction band is associated with the contribution of valence electrons of Mg s, Mg p, Zn s and Zn p orbitals. It is worth noting that there is a peak at -7 eV, which is mainly provided by the valence electrons of the Zn d orbital. In addition, there is sp hybridization between Mg s–Mg p and Zn s–Zn p orbitals in the valence band. Figure 6 shows that the bonding peaks in $\text{Mg}_{52}\text{Ag}_2$ are mainly distributed between -6.5 and 2 eV. Here, the valence band is associated with the valence electrons of the Mg s, Mg p, Ag s, Ag p and Ag d orbitals, and the conduction band is mostly associated with the valence electrons of Mg s and Mg p orbitals. Overall, the contribution of the Ag s and Ag p orbital is limited. There is a peak at -4.5 eV, which is mainly contributed by the valence electrons of the Ag d orbital. At the same time, the density of states of the Ag d orbital overlaps with those of other orbitals in the entire valence band range, indicating the presence of spd hybridization amongst Mg s, Mg p, and Ag d orbitals. In general, the density of state of $\text{Mg}_{52}\text{Ag}_2$ at the Fermi level is higher than that of $\text{Mg}_{52}\text{Zn}_2$, which shows more active metallicity. In addition, the hybridization of $\text{Mg}_{52}\text{Ag}_2$ is also more pronounced than that of $\text{Mg}_{52}\text{Zn}_2$.

3.3.2. Electron Density Difference

In order to reveal the mechanism of the strengthening effect of Zn and Ag on a Mg-based alloy, the electron density differences of Mg_{54} , $Mg_{52}Zn_2$ and $Mg_{52}Ag_2$ have been calculated and analyzed. Usually, the electron density difference can be used to analyze the electron transfer between atoms in the crystal structures. At the same time, the state of bonding in the crystal structures can also be assessed using an electron density difference diagram. The electron density difference diagrams of Mg_{54} , $Mg_{52}Zn_2$ and $Mg_{52}Ag_2$ are shown in Figure 7. It can be seen from Figure 7 that the electron clouds around each nucleus in Mg_{54} , $Mg_{52}Zn_2$ and $Mg_{52}Ag_2$ are uniformly and clearly distributed, and there are no obvious overlaps between electron clouds. This indicates that in the structures of Mg_{54} , $Mg_{52}Zn_2$ and $Mg_{52}Ag_2$, the atoms bond with each other through metallic bonds. From Figure 7, charge accumulation can be seen around the nuclei of Mg, Zn, and Ag atoms, but the scales of the color cards in the three color maps are different. In the scaling of the color card, the reddest area (at the bottom) indicates the maximum charge density. It can be found that the maximum charge density of Mg_{54} is $2.425 \times 10^{-2} e/\text{\AA}^3$, the maximum charge density of $Mg_{52}Zn_2$ is $5.247 \times 10^{-2} e/\text{\AA}^3$, and the maximum charge density of $Mg_{52}Ag_2$ is $1.047 \times 10^{-1} e/\text{\AA}^3$. It is clear that $Mg_{52}Zn_2$ and $Mg_{52}Ag_2$ aggregate more electrons in their bonding regions than Mg_{54} , indicating that the addition of Zn and Ag atoms can enhance the stability of the matrix. In addition, $Mg_{52}Ag_2$ aggregates more electrons in the bonding region than $Mg_{52}Zn_2$, indicating that Ag atoms have a stronger capacity to promote the stability of the matrix than Zn atoms. This also corresponds to previous calculations and the results of the analysis of cohesive energies and tensile properties from an electronic perspective, indicating that the previous analysis results are correct.

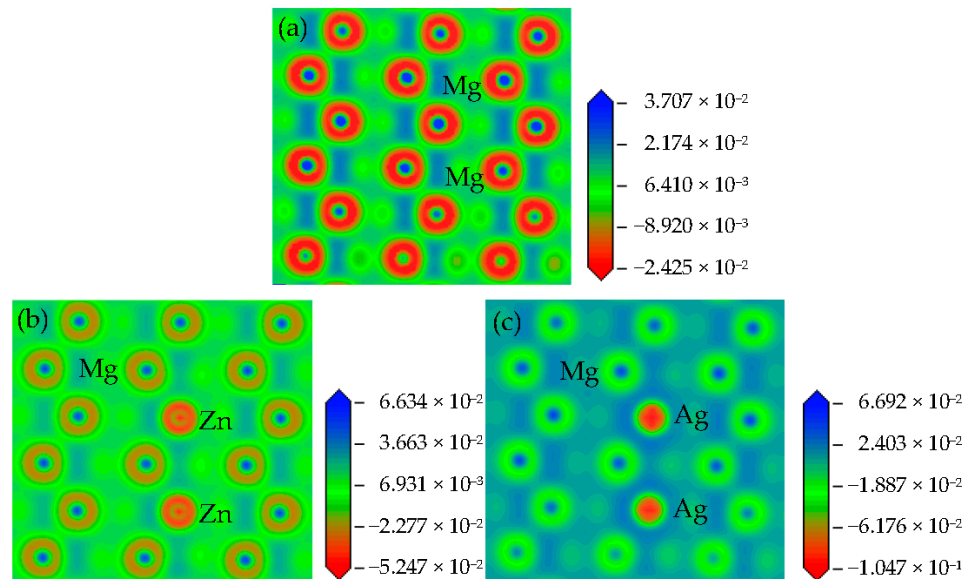


Figure 7. Electron density differences of Mg_{54} (a), $Mg_{52}Zn_2$ (b) and $Mg_{52}Ag_2$ (c).

4. Conclusions

In this work, the structural, electronic and tensile properties of the solid solution structures of Mg_{54} , $Mg_{53}X_1$ and $Mg_{52}X_2$ ($X = Zn, Ag$) subjected to 0–20% strains are investigated using the first principle calculation method. The conclusion is that the solid solution structures of $Mg_{53}X_1$ and $Mg_{52}X_2$ ($X = Zn, Ag$) are stable in the 0–20% strain range. In addition, the stability of the Ag structures is greater than that of the Zn structures when two levels of solid solubility are employed. With the increase in strains, several solid solution structures at these two levels of solid solubility show obvious yielding. The results show that the application of both Zn and Ag can increase the yield strength of Mg-based alloys. The strengthening effect of Zn is more obvious. In addition, the strengthening effect is also affected by the solution's concentration. When the solubility is 3.7 at.%, the

strengthening effect is greater. The stress–strain results of tensile strength show that Zn does not promote the tensile strength of Mg-based alloys, while Ag can improve the tensile strength. The strengthening effect is strong at a solubility level of 3.7 at.%, compared to 1.8 at.%. Finally, the analyses of the density of states and the electron density difference verify the mechanisms of the strengthening effects of elements Zn and Ag on Mg-based alloys from the electronic perspective.

Author Contributions: Writing—original draft preparation, Y.G.; revising W.F.; writing—review and editing, L.F. and C.W.; project administration, Y.G. and X.C. All authors have read and agreed to the published version of the manuscript.

Funding: This study was funded by the Natural Science Foundation of Liaoning Province (Nos. 2021-BS-156 and 2021-BS-154), the Ministry of Education industry-school cooperative education project (Nos. 220606517061413, 220502116230206 and 220606517061317), the Graduate Education and Teaching Reform Project of Shenyang Normal University (No. YJSJG320210102), the ninth batch of teaching reform project of Shenyang Normal University (No. JG2021-YB063), and Innovative Talent Program of Shenyang Normal University, grant number 222-51300417.

Institutional Review Board Statement: Not applicable.

Informed Consent Statement: Not applicable.

Data Availability Statement: Not applicable.

Conflicts of Interest: The authors declare no conflict of interest.

References

1. Xie, J.; Zhang, J.; You, Z.; Liu, S.; Guan, K.; Wu, R.; Wang, J.; Feng, J. Towards developing Mg alloys with simultaneously improved strength and corrosion resistance via RE alloying. *J. Magnes. Alloys* **2021**, *9*, 41–56. [\[CrossRef\]](#)
2. Sharma, S.K.; Saxena, K.K.; Malik, V.; Mohammed, K.A.; Prakash, C.; Buddhi, D.; Dixit, S. Significance of Alloying Elements on the Mechanical Characteristics of Mg-Based Materials for Biomedical Applications. *Crystals* **2022**, *12*, 1138. [\[CrossRef\]](#)
3. Ji, H.; Liu, W.; Wu, G.; Ouyang, S.; Gao, Z.; Peng, X.; Ding, W. Influence of Er addition on microstructure and mechanical properties of as-cast Mg-10Li-5Zn alloy. *Mater. Sci. Eng. A* **2019**, *739*, 395–403. [\[CrossRef\]](#)
4. Tian, Y.; Hu, H.J.; Zhao, H.; Zhang, W.; Liang, P.C.; Jiang, B.; Zhang, D.F. An extrusion–shear–expanding process for manufacturing AZ31 magnesium alloy tube. *Trans. Nonferrous Met. Soc. China* **2022**, *32*, 2569–2577. [\[CrossRef\]](#)
5. Wang, G.G.; Weiler, J.P. Recent developments in high-pressure die-cast magnesium alloys for automotive and future applications. *J. Magnes. Alloys* **2023**, *11*, 78–87. [\[CrossRef\]](#)
6. Liu, J.; Sun, J.; Chen, Q.; Lu, L. Intergranular Cracking in Mg-Gd-Y Alloy during Tension Test. *Crystals* **2022**, *12*, 1040. [\[CrossRef\]](#)
7. Wang, M.; Xu, X.Y.; Wang, H.Y.; He, L.H.; Huang, M.X. Evolution of dislocation and twin densities in a Mg alloy at quasi-static and high strain rates. *Acta Mater.* **2020**, *201*, 102–113. [\[CrossRef\]](#)
8. Du, H.Q.; Li, F.; Huo, P.D.; Wang, Y. Microstructure evolution and ductility improvement mechanisms of magnesium alloy in interactive alternating forward extrusion. *Trans. Nonferrous Met. Soc. China* **2022**, *32*, 2557–2568. [\[CrossRef\]](#)
9. Guo, P.C.; Li, L.C.; Liu, X.; Ye, T.; Cao, S.F.; Xu, C.C.; Li, S.K. Compressive deformation behavior and microstructure evolution of AM80 magnesium alloy under quasi-static and dynamic loading. *Int. J. Impact. Eng.* **2017**, *109*, 112–120. [\[CrossRef\]](#)
10. Pan, F.S.; Mao, J.J.; Zhang, G.; Tang, A.; She, J. Development of high-strength, low-cost wrought Mg–2.0 mass% Zn alloy with high Mn content. *Prog. Nat. Sci.-Mater.* **2016**, *26*, 630–635. [\[CrossRef\]](#)
11. Jiang, B.; Dong, Z.H.; Zhang, A.; Song, J.F.; Pan, F.S. Recent advances in micro-alloyed wrought magnesium alloys: Theory and design. *Trans. Nonferrous Met. Soc. China* **2022**, *32*, 1741–1780. [\[CrossRef\]](#)
12. Huang, W.S.; Chen, J.H.; Yan, H.G.; Li, Q.; Xia, W.J.; Su, B.; Zhu, W.J. Solid solution strengthening and damping capacity of Mg–Ga binary alloys. *Trans. Nonferrous Met. Soc. China* **2022**, *32*, 2852–2865. [\[CrossRef\]](#)
13. Miao, J.S.; Sun, W.H.; Klarner, A.D.; Luo, A.A. Interphase boundary segregation of silver and enhanced precipitation of Mg₁₇Al₁₂ Phase in a Mg–Al–Sn–Ag alloy. *Scr. Mater.* **2018**, *154*, 192–196. [\[CrossRef\]](#)
14. Cáceres, C.H.; Blake, A. The Strength of Concentrated Mg–Zn Solid Solutions. *Phys. Status Solidi A* **2002**, *194*, 147–158. [\[CrossRef\]](#)
15. Wang, J.F.; Wang, K.; Hou, F.; Liu, S.J.; Peng, X.; Wang, J.X.; Pan, F.S. Enhanced strength and ductility of Mg–RE–Zn alloy simultaneously by trace Ag addition. *Mater. Sci. Eng. A* **2018**, *728*, 10–19. [\[CrossRef\]](#)
16. Tong, L.B.; Li, X.H.; Zhang, H.J. Effect of long period stacking ordered phase on the microstructure, texture and mechanical properties of extruded Mg–Y–Zn alloy. *Mater. Sci. Eng. A* **2013**, *563*, 177–183. [\[CrossRef\]](#)
17. Giusepponi, S.; Celino, M. The ideal tensile strength of tungsten and tungsten alloys by first-principles calculations. *J. Nucl. Mater.* **2013**, *435*, 52–55. [\[CrossRef\]](#)
18. Roundy, D.; Cohen, M.L. Ideal strength of diamond, Si, and Ge. *Phys. Rev. B* **2001**, *64*, 212103. [\[CrossRef\]](#)

19. Luo, W.D.; Roundy, D.; Cohen, M.L.; Morris, J.W. Ideal strength of bcc molybdenum and niobium. *Phys. Rev. B* **2002**, *66*, 094110. [[CrossRef](#)]
20. Lu, G.H.; Deng, S.H.; Wang, T.M.; Kohyama, M.; Yamamoto, R. Theoretical tensile strength of an Al grain boundary. *Phys. Rev. B* **2004**, *69*, 134106. [[CrossRef](#)]
21. Zhang, Y.; Lü, G.H.; Deng, S.H.; Wang, T.M. First-principles computational tensile test on an Al grain boundary. *Acta Phys. Sin-Ch. Ed.* **2006**, *55*, 2901–2907. (In Chinese) [[CrossRef](#)]
22. Liu, X.; Liu, Z.; Liu, G.; Wang, W.; Li, J. First-principles study of solid solution strengthening in Mg–X (X=Al, Er) alloys. *Bull. Mater. Sci.* **2019**, *42*, 16. [[CrossRef](#)]
23. Luo, S.Q.; Tang, A.T.; Pan, F.S.; Song, K.; Wang, W.Q. Effect of mole ratio of Y to Zn on phase constituent of Mg–Zn–Zr–Y alloys. *Trans. Nonferrous Met. Soc. China* **2011**, *21*, 795–800. [[CrossRef](#)]
24. Wang, C.; Han, P.D.; Zhang, L.; Zhang, C.L.; Yan, X.; Xu, B.S. The strengthening effect of Al atoms into Mg–Al alloy: A first-principles study. *J. Alloys Compd.* **2009**, *482*, 540–543. [[CrossRef](#)]
25. Wang, C.; Huang, T.L.; Wang, H.Y.; Xu, X.N.; Jiang, Q.C. Effects of distributions of Al, Zn and Al+Zn atoms on the strengthening potency of Mg alloys: A first-principles calculations. *Comput. Mater. Sci.* **2015**, *104*, 23–28. [[CrossRef](#)]
26. Gironcoli, S.D.; Baroni, S.; Resta, R. Piezoelectric properties of III-V semiconductors from first-principles linear-response theory. *Phys. Rev. Lett.* **1989**, *62*, 2853–2856. [[CrossRef](#)]
27. Ganeshan, S.; Shang, S.L.; Wang, Y.; Liu, Z.K. Effect of alloying elements on the elastic properties of Mg from first-principles calculations. *Acta Mater.* **2009**, *57*, 3876–3884. [[CrossRef](#)]
28. Batchelder, F.W.; Raeluechle, R.F. Lattice Constants and Brillouin Zone Overlap in Dilute Magnesium Alloys. *Phys. Rev. B* **1957**, *105*, 59–61. [[CrossRef](#)]
29. Zhang, C.; Han, P.; Li, J.; Chi, M.; Yan, L.; Liu, Y.; Liu, X.; Xu, B. First-principles study of the mechanical properties of NiAl microalloyed by M (Y, Zr, Nb, Mo, Tc, Ru, Rh, Pd, Ag, Cd). *J. Phys. D Appl. Phys.* **2008**, *41*, 095410. [[CrossRef](#)]
30. Mao, P.L.; Yu, B.; Liu, Z.; Wang, F.; Ju, Y. Mechanical, electronic and thermodynamic properties of Mg₂Ca Laves phase under high pressure: A first-principles calculation. *Comput. Mater. Sci.* **2014**, *88*, 61–70. [[CrossRef](#)]
31. Wang, F.; Sun, S.J.; Wang, Z.; Yu, B.; Mao, P.L.; Liu, Z. Microstructure, mechanical properties and first-principle analysis of vacuum die-cast Mg–7Al alloy with Sn addition. *Rare Metals* **2015**, *41*, 1961–1967. [[CrossRef](#)]
32. Mao, P.L.; Yu, B.; Liu, Z.; Wang, F.; Ju, Y. First-principles calculations of structural, elastic and electronic properties of AB₂ type intermetallics in Mg–Zn–Ca–Cu alloy. *J. Magnes. Alloys* **2013**, *1*, 256–262. [[CrossRef](#)]
33. Li, C.; Zhang, K.; Ru, J.G. Pressure dependence of structural, elastic and electronic of Mg₂Y: A first principles study. *J. Alloys Compd.* **2015**, *647*, 573–577. [[CrossRef](#)]
34. Feng, Y.; Zhu, S.; Wang, L.; Chang, L.; Hou, Y.; Guan, S. Fabrication and characterization of biodegradable Mg–Zn–Y–Nd–Ag alloy: Microstructure, mechanical properties, corrosion behavior and antibacterial activities. *Bioact. Mater.* **2018**, *3*, 225–235. [[CrossRef](#)] [[PubMed](#)]
35. Ben-Hamu, G.; Eliezer, D.; Kaya, A.; Na, Y.G.; Shin, K.S. Microstructure and corrosion behavior of Mg–Zn–Ag alloys. *Mater. Sci. Eng. A* **2006**, *5*, 579–587. [[CrossRef](#)]
36. Zhao, H.; Wang, L.Q.; Ren, Y.P.; Yang, B.; Li, S.; Qin, G.W. Microstructure, Mechanical Properties and Corrosion Behavior of Extruded Mg–Zn–Ag Alloys with Single-Phase Structure. *Acta Metall. Sin. (Engl. Lett.)* **2018**, *31*, 575–583. [[CrossRef](#)]

Disclaimer/Publisher’s Note: The statements, opinions and data contained in all publications are solely those of the individual author(s) and contributor(s) and not of MDPI and/or the editor(s). MDPI and/or the editor(s) disclaim responsibility for any injury to people or property resulting from any ideas, methods, instructions or products referred to in the content.